# Large-scale molecular dynamics simulations of high energy cluster impact on a diamond surface

## 2nd report: Impact-induced crater and shockwave

Y. Yamaguchi[1,a], J. Gspann[2], and T. Inaba[1]

[1] Department of Mechanophysics Engineering, Osaka University, 2-1 Yamadaoka, Suita, Osaka 565-0871, Japan
[2] Institut für Mikrostrukturtechnik, Universität und Forschungszentrum Karlsruhe, Postfach 3640, 76021 Karlsruhe, Germany

**Abstract.** Large-scale molecular dynamics simulations of high acceleration energy single cluster impacts on a diamond surface are performed in order to investigate the cluster surface interaction. The formation of the crater and of the multiple shockwaves at a cluster acceleration energy $E_a = 100$ keV is studied in detail in this report. The two $Ar_{961}$ impact simulations using and not using external symmetric region do not show any clear difference, so that the unspherical crater structure at the very beginning of the impact and the shockwave propagation directions do not result from the respective outer region representation but from the effect of the crystal structure of diamond. The impact simulation of a virtual hard spherical cluster demonstrates a deeper transient crater as well as a more pronounced final impact morphology while the impact-induced multi-layered shockwaves resemble those seen in the case of the normal cluster impact.

## 1 Introduction

Atomic or molecular cluster beams are considered as a useful tool for surface modification including deposition, ion implantation, polishing, and chemical and physical erosion [1,2]. The authors' group has used highly accelerated ionized cluster beams as the erosion source for the purpose of nano- and micro-scale surface structuring [3–5]. Here, clusters consisting of about 1000 $CO_2$ or argon molecules are accelerated up to 100 keV, and very smooth eroded surfaces were obtained with continuous impacts for various materials ranging from Teflon, silicon, glass, and diamond, and this technique has thus a potential as a direct micro-fabrication tool.

The authors have also performed large-scale molecular dynamics (MD) simulations of single $Ar_n$ or $(CO_2)_n$ ($n \simeq$ 960) cluster impacts on a diamond (111) surface [6,7]. For a cluster impact energy $E_a$ of 100 keV/cluster, the formation of a hemispherical crater and two or three-layered induced shockwaves were observed at the early stage of the impact process. Rebounding hot fluidized carbon material was then seen to replenish the transient crater very quickly until 2 ps, with a central peak appearing as a long time phenomenon only in the case of a $CO_2$ impact. Transient craters developed also for lower impact energies

of $30 \leq E_a \leq 75$ keV while only an elastic deformation was seen for $E_a = 10$ keV. The volume of the transient crater was approximately proportional to $E_a$ while the volume of the plastically deformed region and the kinetic energy transfer *via* the shockwave were linear functions of $E_a$ minus a threshold energy of about 10 keV. At an impact energy of 100 keV, the number of carbon atoms emitted from the target was much larger for a $CO_2$ cluster impact than for an argon cluster impact with a factor of about 3.35. The reactive enhancement of the surface erosion in the $CO_2$ case was also proven by a strong CO signal in the spectrum of the emitted fragments. On the other hand, the surface of the relaxed crater was more densely packed and smoother in the case of the argon cluster impact.

Although these results do not seem to depend on the particular boundary condition using the external symmetric region [6,7], the structure of the crater at the very beginning after the first 0.3 ps and the induced shockwave showed unspherical aspects. It has been argued that these features may result from the chosen boundary conditions, in particular from simulating only 1/6 of the external region in detail. It is also not clear why the unusual multi-layered shockwaves are formed – due to the deformation of the impact cluster, or other factors –. In this report, single argon cluster impacts with an acceleration energy $E_a$ of 100 keV are simulated without the restriction to the specific 1/6 "symmetric" external region chosen in the

[a] e-mail: `yamaguchi@mech.eng.osaka-u.ac.jp`

**Table 1.** Interaction potential parameters between undeformable spherical particle and carbon.

| $\varepsilon_{\text{Ar-C}}$ (J) | $\sigma_{\text{Ar-C}}$ (Å) | $\rho_n$ (1/Å$^3$) | $R$ (Å) |
|---|---|---|---|
| $8.013 \times 10^{-22}$ | 3.385 | $1.468 \times 10^{-2}$ | 25 |

previous calculations. In addition, the impact process of a single spherical particle which mimics an undeformable hard spherical cluster is also simulated and compared with the normal cluster impact in order to determine the effect of the cluster deformation on the impact-induced crater and shockwave.

## 2 Simulation method

The detail of the calculation is almost the same as in our previous reports [6,7], where the empirical potential function proposed by Brenner [8] is applied for the interaction among carbon atoms, and the 12-6 Lennard-Jones potential is adopted for Ar-C and Ar-Ar interactions [6,7].

In addition to the normal cluster impact, an undeformable spherical particle impact is considered in this report. Assuming that argon atoms are homogeneously distributed in the particle, the interaction potential between the particle and a carbon with a distance $r$ from the center of the sphere can be expressed as an integrated form as follows:

$$\Phi(r) = \rho_n \int_0^R \mathrm{d}s \int_0^\pi 2\pi s^2 \sin\theta \mathrm{d}\theta \phi \left( \sqrt{r^2 - 2rs\cos\theta + s^2} \right) \tag{1}$$

where $R$, $\rho_n$, and $\phi$ denote the radius of the particle, the number density of argon atoms, and the atom-atom interaction potential between argon and carbon as a function of the distance, respectively. Then, the integrated potential $\Phi$ is written as in equation (2) applying the 12-6 Lennard-Jones potential for $\phi$ with the interaction parameters $\varepsilon_{\text{Ar-C}}$ and $\sigma_{\text{Ar-C}}$.

$$\Phi(r) = \frac{4\pi\rho_n\sigma^3\epsilon}{3r} \left[ \frac{1}{15} \left[ R \left\{ \left( \frac{\sigma}{r-R} \right)^9 + \left( \frac{\sigma}{r+R} \right)^9 \right\} \right. \right.$$
$$+ \frac{\sigma}{8} \left\{ \left( \frac{\sigma}{r-R} \right)^8 + \left( \frac{\sigma}{r+R} \right)^8 \right\} \right]$$
$$- \frac{1}{2} \left[ R \left\{ \left( \frac{\sigma}{r-R} \right)^3 + \left( \frac{\sigma}{r+R} \right)^3 \right\} \right.$$
$$\left. \left. + \frac{\sigma}{2} \left\{ \left( \frac{\sigma}{r-R} \right)^2 + \left( \frac{\sigma}{r+R} \right)^2 \right\} \right] \right] \tag{2}$$

The potential parameters are shown in Table 1, where the values of $R$ and $\rho_n$ are derived from the normal argon impact cluster Ar$_{961}$ [6,7], and the mass of the particle is the same as Ar$_{961}$.

The diamond (111) impact target with the external symmetric region is the same as in our previous report [6,7], consisting of a hexagonal internal full-simulated

surface region and a surrounding symmetric external region. Only 1/6 of the external region is simulated, and its symmetric images are connected with the internal region to reduce the calculation time. The internal and external regions contain 758 440 and 308 240 carbon atoms, respectively (2 584 741 carbon atoms including virtual images). The vertical depth and the length of the diagonal line of the internal region are about 115 Å and 122 Å respectively, and the external region extends by another 50% of the symmetric region. The outer boundary of the external region is fixed and the temperature is controlled at 300 K near the outer boundary with the Langevin method. The target without the external symmetric region consists of 2 365 650 carbon atoms where symmetric images are only adopted for the fixed outer boundary, and the total number of carbon atoms including virtual images are the same.

The simulations were carried out with the VPP5000 at the Forschungszentrum Karlsruhe.

## 3 Results and discussions

### 3.1 Effect of the external symmetric region

Figure 1 shows the comparison of Ar$_{961}$ cluster impacts with an acceleration energy $E_a$ of 100 keV using and not using the external symmetric region until 1 ps after the impact. A cross-section parallel to the impact direction with a thickness of 10 Å is shown here, and carbon atoms with larger velocity have darker shade. The crater and shockwave structures are almost completely the same during the whole process in Figure 1, and therefore, the unspherical structures of the crater after the first 0.3 ps [Figs. 1(a1, b1)] and the particular propagation directions of the induced shockwaves are not to be attributed to the side-effect of external symmetric region but to the effect of the crystal structure of diamond. The structures of the shockwaves in the external region are also well reproduced at 1.0 ps [Fig. 1(a3)], showing again the applicability of the external symmetric region.

### 3.2 Hard particle impact

Figure 2 shows the snapshots of a hard particle impact using the integrated potential function described in Section 2 with an acceleration energy $E_a$ of 100 keV (10 Å cross-section), where the depicted impact particle is not exactly on scale. The shockwaves propagate earlier [Figs. 2(a–c)] than in the case of the normal argon cluster impact shown in Figures 1(a–c), and therefore, the first shockwave-front for the normal cluster impact is considered to be generated not just at the first contact with the surface but after a small time lag. Two or three layered shockwaves are however generated for both impacts, and these structures themselves are very similar to each other including the distance between two parallel shockwaves, showing that the multi-layered shockwaves are at least not due to the cluster deformation. The transient crater is replenished by the rebounding hot fluidized carbon material before 3 ps
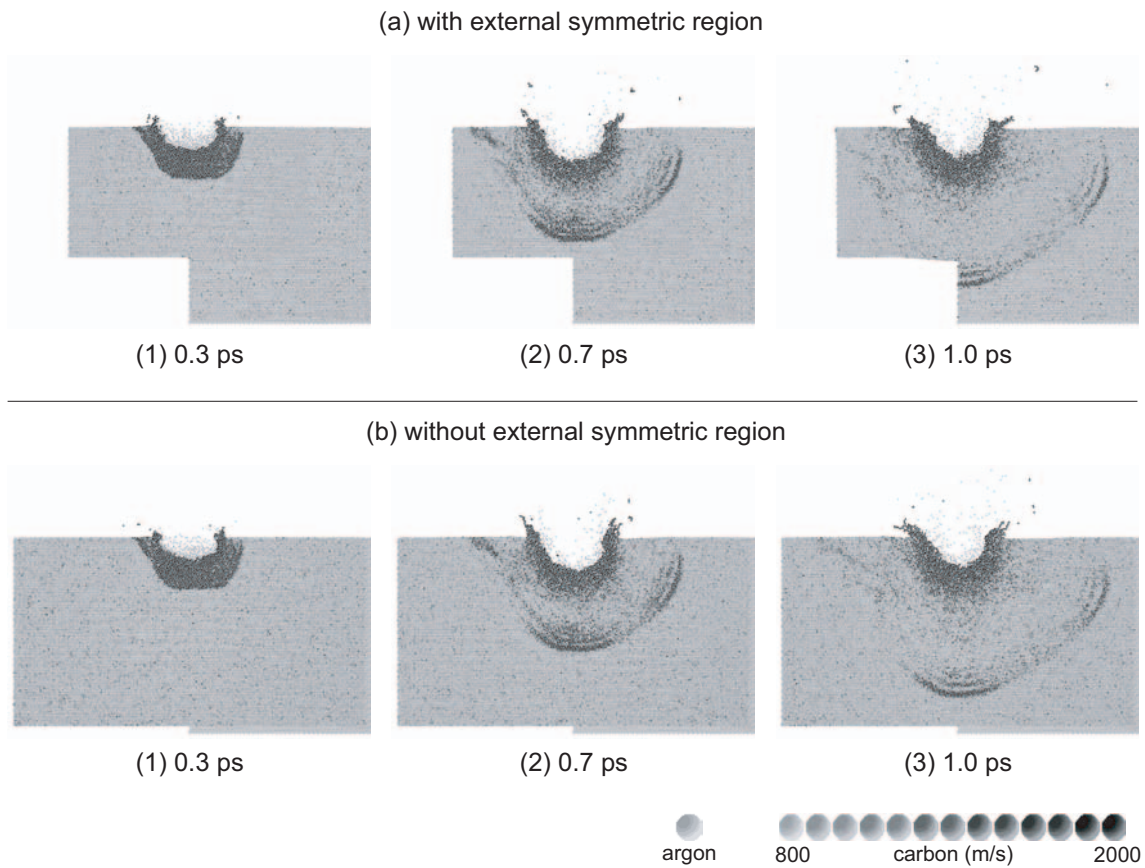
(a) with external symmetric region



(1) 0.3 ps                    (2) 0.7 ps                    (3) 1.0 ps

(b) without external symmetric region



(1) 0.3 ps                    (2) 0.7 ps                    (3) 1.0 ps

argon        800        carbon (m/s)        2000

**Fig. 1.** Comparison of $Ar_{961}$ cluster impacts using and not using the external symmetric region with an acceleration energy $E_a$ of 100 keV (10 Å cross-section).



(a) 0.3 ps                    (b) 0.7 ps                    (c) 1.0 ps



(d) 1.5 ps                    (e) 2.0 ps                    (f) 3.0 ps
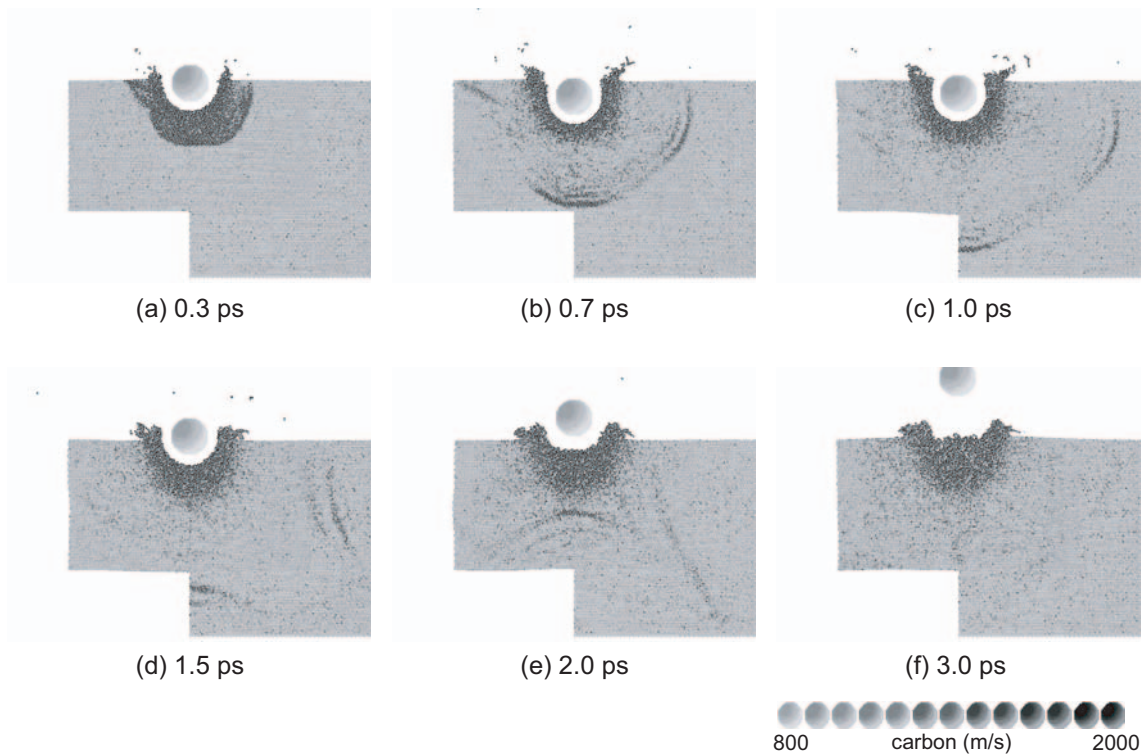
800        carbon (m/s)        2000

**Fig. 2.** Snapshots of a hard particle impact using the integrated potential function with an acceleration energy $E_a$ of 100 keV (10 Å cross-section). The depicted impact particle is not exactly on scale.
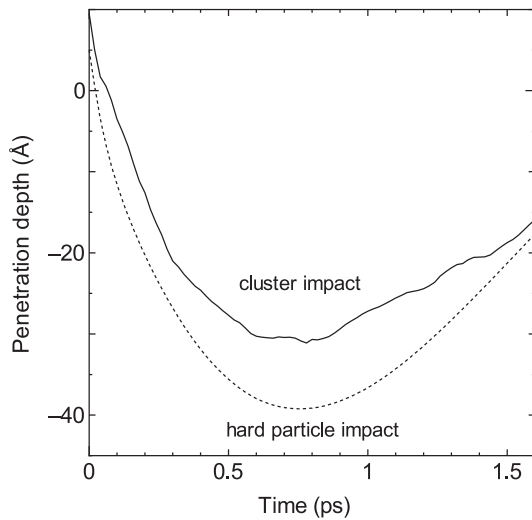
cluster resulted also in a larger penetration depth [9], but the significance of the parameters is not yet clear.

## 4 Concluding remarks

Large-scale molecular dynamics simulations with high acceleration energy cluster impact on a diamond surface were performed in order to investigate the cluster surface interaction. The formation of the crater and the shockwaves at a cluster acceleration energy $E_a = 100$ keV was studied in detail. The two $Ar_{961}$ impact simulations using and not using an external symmetric region indicated no clear difference and the unspherical crater structure at beginning and the shockwave propagation directions were ascribed to the effect of the crystal structure of diamond. The impact using a virtual undeformable hard spherical cluster showed a rather different cratering morphology while similar multi-layered shockwave structures were observed.

## References

1. J. Gspann, Sensors Actuat. A **51**, 37 (1995)
2. D.B. Fenner *et al.*, Mat. Res. Soc. Symp. Proc. **585**, 27 (2000)
3. A. Gruber, J. Gspann, H. Hoffmann, Appl. Phys. A **68**, 197 (1999)
4. C. Becker, J. Gspann, R. Krämer, Eur. Phys. J. D **16**, 301 (2001)
5. C. Becker *et al.*, Chin. Phys. **10**, 174 (2001)
6. Y. Yamaguchi, J. Gspann, Eur. Phys. J. D **16**, 105 (2001)
7. Y. Yamaguchi, J. Gspann, Phys. Rev. B **66**, 155408 (2002)
8. D.W. Brenner, Phys. Rev. B **42**, 9458 (1992)
9. Y. Yamaguchi, J. Gspann, unpublished data

**Fig. 3.** Time series of the penetration depths of the argon cluster and the hard spherical particle.

[Fig. 2(d)], as well as in the case of the normal cluster impact [6,7] though the crater rim structure is much larger and distinct for the particle impact, and it seems more similar to a meteor impact crater.

Figure 3 shows the time series of the penetration depths of the argon cluster in Figure 1 and the hard spherical particle in Figure 2. In the latter case, the depth of penetration is given by the vertical position of the center of mass of the spherical particle, increased by its radius $R$. The hard particle penetrates deeper than the argon cluster, and the maximum penetration depth at about $0.7 \sim 0.8$ ps is about 10 Å larger, however, the time at the maximum penetration depth and the returning time, *i.e.* the two penetration profiles look similar. The difference in the penetration depth may be due to the backward expansion shockwave inside the impact cluster which reduces the impact moment on the surface. A simulation using heavy molecule with the same impact energy as the